Microwave-assisted preparation of manganese dioxide modified activated carbon for adsorption of lead ions

Heng Yan, Wenhai Hu, Song Cheng, Hongying Xia, Quan Chen, Libo Zhang and Qi Zhang

ABSTRACT

In this study, manganese dioxide was evenly distributed on the surface of activated carbon (AC), and the porous structure of AC and the surface functional groups of manganese dioxide were used to adsorb the heavy metal ion Pb(II). The advantages of microwave heating are fast heating and high selectivity. The mole ratio control of the AC and MnO_2 in 1:0.1, microwave heating to 800 °C, heat preservation for 30 min. The maximum adsorption capacity of the MnO_2-AC prepared by this method on Pb(II) can reach 664 mg/L at pH = 6. It can be observed by scanning electron microscope (SEM) that manganese dioxide particles are dispersed evenly on the surface and pore diameter of AC, and there is almost no agglomeration. The specific surface area was 752.8 m^2/g, and the micropore area was 483.9 m^2/g. The adsorption mechanism was explored through adsorption isotherm, adsorption kinetics, Fourier transform infrared spectroscopy (FTIR), X-ray diffraction (XRD), X-ray photoelectron spectroscopy (XPS). It is speculated that the adsorption mechanism includes electrostatic interaction and specific adsorption, indicating that lead ions enter into the void of manganese dioxide and form spherical complexes. The results showed that the adsorption behavior of Pb(II) by MnO_2-AC was consistent with the Langmuir adsorption model, the quasi-second-order kinetic model, and the particle internal diffusion model.

Key words | activated carbon, adsorption, lead ions, microwave heating, MnO_2-AC

Heng Yan
Wenhai Hu
Song Cheng
Hongying Xia (corresponding author)
Quan Chen
Libo Zhang
Qi Zhang
State Key Laboratory of Complex Nonferrous Metal Resources Clean Utilization,
Kunming University of Science and Technology,
Kunming, Yunnan 650093,
China;
The Key Laboratory of Unconventional Metallurgy, Ministry of Education,
Kunming University of Science and Technology,
Kunming, Yunnan 650093,
China;
and
Faculty of Metallurgical and Energy Engineering,
Kunming University of Science and Technology,
Kunming, Yunnan 650093,
China
E-mail: *hyxia81@163.com*

HIGHLIGHTS

- The addition of MnO_2 improves the adsorption performance of activated carbon on lead ions, and solves the problem of greatly reduced adsorption efficiency due to flocculation when MnO_2 is used alone.
- Microwave heating method is easier to control the beginning and end of heating.
- MnO_2-AC has a good adsorption effect on lead ions and can have application in industrial production.

GRAPHICAL ABSTRACT

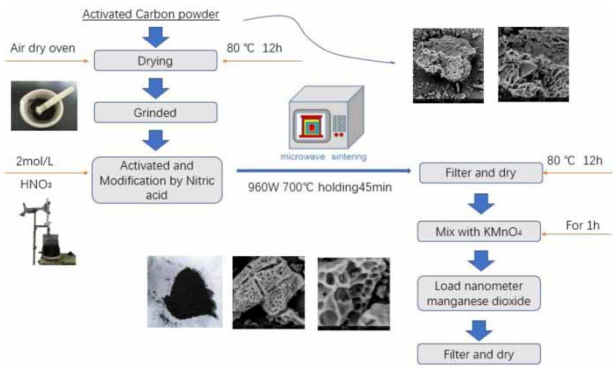

doi: 10.2166/wst.2020.350

INTRODUCTION

Industrial wastewater contains many kinds of heavy metals, such as Cr, Pb, Cu, Cd, and so on, which are considered to be persistent, bioaccumulative and harmful substances (Manes & Hofer 1982; Chansuvarn & Jainae 2017; Mallakpour & Motirasoul 2018). As far as the current development is concerned, although various wastewater treatment technologies can be applied, some of the wastewater will be directly or indirectly discharged into the environment. Besides, the presence of heavy metals poses serious threat to ecological environment security due to their higher concentration and strong mobility in the environment (Mishra *et al.* 2004; Peng *et al.* 2015). Langmuir (1917) mentioned that fractions of heavy metals in the environment include exchangeable, weak acid-soluble fractions, reducible fractions, oxidizable fractions and residual fractions. In addition, exchangeable fractions and weak acid soluble fractions were regarded as bioavailable metal fractions; that is, unstable fractions, which can be absorbed by microbes and plants, and finally concentrated in the human body through the food chain. They combine with many substances in the environment to form complexes, which can migrate and transform in the water body and greatly increase solubility, thereby causing secondary pollution (Pera-Titus *et al.* 2004; Pourjavid *et al.* 2014). What is noteworthy is that reducing the heavy metals concentration and converting from unstable fractions to stable fractions may do well in weakening their risk (Mishra *et al.* 2004).

Now, various remediation technologies have been developed for metals removal from wastewaters (Tangahu *et al.* 2011; Khushk *et al.* 2020). Common methods for handling heavy metal ions include a biological method, chemical deposition, redox method, osmotic filtration method and adsorption method (Manes & Hofer 1982; Chansuvarn & Jainae 2017). Adsorption is the most economical, widely available and effective method for which activated carbon is the adsorbent of choice. Therefore, it is of great significance to develop an efficient adsorbent for wastewater treatment.

Multiple researches have shown that manganese dioxide has better adsorption performance, and its unique octahedral structure can absorb heavy metal ions. Hydrated manganese dioxide is a kind of manganese oxide commonly used in water treatment; nevertheless, the particles have the disadvantage of easy condensation, and the average particle size is 80 nm (Tangahu *et al.* 2011; Wan *et al.* 2016; Mallakpour & Motirasoul 2018). The easy agglomeration of manganese dioxide will cause its adsorption effect to be greatly reduced. Although the adsorption effect of activated carbon on lead ions is improved, the activated carbon is modified with nitric acid and doped with manganese dioxide. The loading of manganese dioxide on activated carbon can also avoid the defects of condensation (Mishra *et al.* 2004; Peng *et al.* 2015; Sellaoui *et al.* 2019).

Manganese dioxide has a relatively high specific surface area and a strong affinity for heavy metal ions plays an important role in the adsorption process (Langmuir 1917; Pera-Titus *et al.* 2004). Compared with other adsorbents, manganese dioxide has a certain selectivity to heavy metals (Pourjavid *et al.* 2014). The new ecological hydrated manganese dioxide studied by S. P. Mishra and colleagues has a minimum particle size of about 10 nm and the largest particle size was 200 nm (Langmuir 1917). This is solved by supporting the MnO_2 on activated carbon, as well as enhancing the adsorption capacity of activated carbon to heavy metal ions (Wang *et al.* 2015, 2017).

In this study, a method for preparing new adsorbent (MnO_2-AC) was proposed. The purpose of this study is to manufacture an adsorbent based on activated carbon with high efficiency to adsorb heavy metal ions. Consequently, the objectives of this work are to: (1) propose a method that through nitric acid modification and microwave heating, can load manganese dioxide on activated carbon. (2) The effects of MnO_2-AC on lead ion adsorption were studied. (3) To explore the adsorption mechanism of MnO_2-AC for lead ions.

MATERIALS AND METHOD

Chemicals

All chemicals in this study are an analytical grade (AR) or better, purchased from Aladdin Industrial Corporation, including activated carbon $KMnO_4$, $MnO_4{\cdot}4H_2O$, HNO_3, etc.

Modification experiment of activated carbon

In order to study the properties of activated carbon before and after modification and the best modification conditions, the following experiments were carried out. Firstly, 1.2 g activated carbon was soaked with different concentrations of nitric acid 200 mL (2 mol/L, 4 mol/L, 6 mol/L, 8 mol/L,10 mol/L). After that, the soaked materials were washed and filtered. Secondly, the material was put into a boxed microwave oven and

heated to 400, 500, 600, 700, and 800 °C with a power of 960 W and kept warm for 30, 45, and 60 min. Finally, after washing and drying, lead ions were adsorbed and compared with unmodified activated carbon to select the optimal modification and heating conditions.

Preparation of manganese dioxide-activated carbon (MnO_2-AC)

MnO_2-AC was synthesized by the coprecipitation method through mixing the $KMnO_4$ and $MnSO_4{\cdot}4H_2O$. The procedures of preparation processing are mainly as follows. Firstly, activated carbon was modified by adding 100 mL nitric acid solution with a concentration of 2 mol/L. After washing and filtering, it was heated to 700 °C with the power of 960 W in the microwave oven and kept warm for 45 min. Secondly, 0.02 mol $KMnO_4$ was made up in a 200 mL solution and mixed with 12 g activated carbon. Activated carbon was allowed to fully absorb potassium permanganate for about 30 min until the solution faded. The $MnSO_4{\cdot}4H_2O$ solution prepared at 0.02 mol was add to a 50 mL burette to control the flow rate. The $MnSO_4{\cdot}4H_2O$ solution was slowly dropped from the burette into a beaker containing activated carbon, which fully adsorbed the $KMnO_4$ and was fully stirred using a magnetic stirring apparatus. Finally, the material was repeatedly washed with ultrapure water 3 times and put into an electrothermal blow dry oven at 80 degree Celsius for 10 h. The dried material will be used for batch sorption experiments and characterization detection. The preparation flow chart is shown in Figure 1.

Batch sorption experiments

Batch sorption experiments were carried out using intermittent testing with powdered MnO_2-AC in a 200 mL conical flask. Typically, the given quality of sorbent (0.02 g) was dispersed into 100 ml Pb(II) solution with a concentration of 100, 150, 200, 250, and 300 mg/L respectively. Adjust the solution pH with HNO_3 and KOH. A thermostatic orbit incubator shaker equipped with gas bath was used to vibrate the flasks at 180 rpm and 298 K taking samples every 20 min for 3 h. After that, samples were taken every 1 h for 6 h. The data was used to investigate the adsorption kinetics. Remaining material was vibrated for 15 h. Preliminary kinetic tests showed that 24 h was sufficient to reach adsorption equilibrium.

Adsorption studies

To evaluate the effect of mass and pH of the novel sorbent, similar batch experiments were performed using different sorbent masses of 5.0, 10.0, 20.0, 40.0, 60.0, 80.0, 100.0, 200.0 and 250.0 mg. In each batch experiment, the adsorption lead ions capacity value was calculated from the

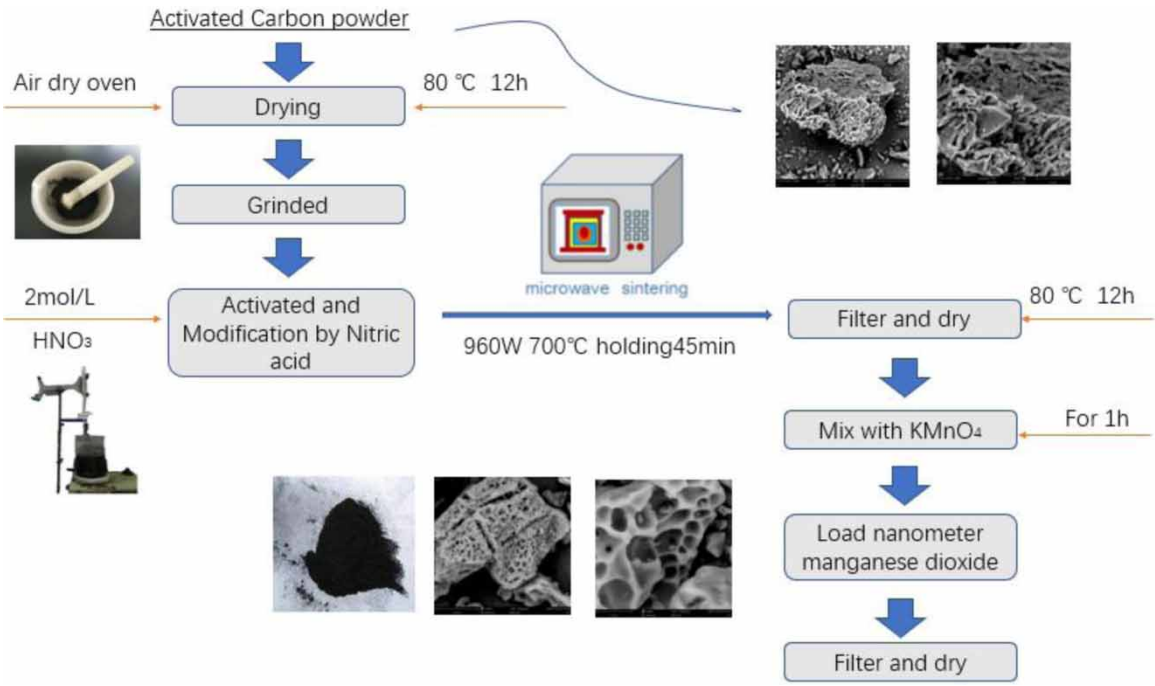

Figure 1 | Preparation of manganese dioxide-activated carbon (MnO_2-AC).

balance q_e.

$$q_t = \frac{C_0 - C_t}{m} V \quad (1)$$

where C_0 and C_t (mol/L) is the initial and residual lead ion concentration respectively, V (L) is the volume of the solution, m (g) is the mass of dry sorbent and q_t (mmol/g) is the sorption capacity of sorbent.

Analytical method

Lead ions concentration in the aqueous phase was analyzed using a TAS-990 flame atom adsorption spectrophotometer (Persee Inc., China), while an atom fluorescence spectrophotometer (AFS-230E) (Haiguang Co., Ltd) was used in other cases. Lead ion solution was prepared by ultrapure water and $Pb(NO_3)_2$ with HNO_3 to be the basic solution.

MnO_2-AC characterization

The surface morphology of the carrier AC and MnO_2 was observed by using a scanning electron microscope (SEM). The crystallinity of the loaded MnO_2 particles was characterized by X-ray diffraction (XRD). The chemical structures of MnO_2-AC and AC were analyzed by Fourier transform infrared spectroscopy (FTIR) over the range of 400–4,000 cm^{-1}. The pore structure properties were determined by an N_2 adsorption-desorption apparatus at 77 K. The specific surface area (S_{BET}) was estimated from N_2 adsorption-desorption data using the Brunauer-Emmett-Teller (BET) equation. The pore distributions were analyzed by Density-Functional-Theory (DFT) method. Energy spectrum analysis was conducted by X-ray photoelectron spectroscopy (XPS) and the original binding energy was adjusted according to the C1s peak. A graphics curve fitting program was used to fit the XPS results.

RESULTS AND DISCUSSION

Dosage ratio of MnO_2-AC

Different mass ratios of manganese dioxide and activated carbon have different adsorption properties. The molar ratio of carbon to manganese dioxide was explored, and the ratio is as follows: C: $MnO_2 = 0.2{:}0.1$; C: $MnO_2 = 0.5{:}0.1$; C: $MnO_2 = 1{:}0.1$; C: $MnO_2 = 1.5{:}0.1$; C: $MnO_2 = 2{:}0.1$. It can be observed in Figure 2 that the adsorption capacity is largest when AC: MnO_2 is 1:0.1. The mass ratio is 12:8.694. The optimal ratio of adsorbed lead ions is 664 mg/g.

When the proportion of MnO_2 increases, there is too much MnO_2 per unit area on the activated carbon, which results in blockage of the activated carbon pores, and manganese dioxide coagulates into agglomerates, thereby reducing the utilization efficiency of the manganese dioxide and

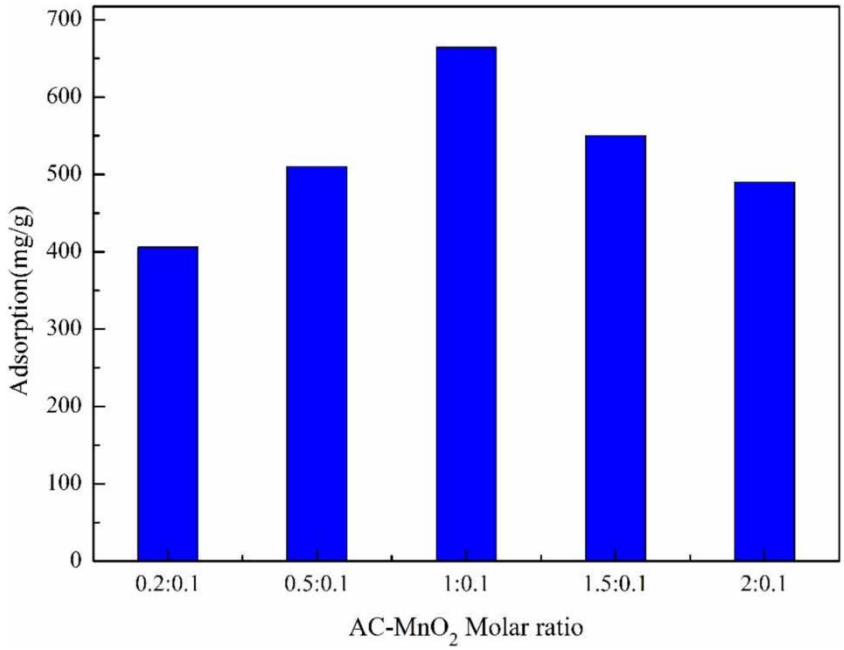

Figure 2 | Molar ratio of AC and MnO_2.

activated carbon. When the ratio of MnO_2 decreases, the binding capacity of manganese dioxide to Pb decreases, resulting in a decrease in the maximum adsorption capacity. Therefore, the ratio 1:0.1 was selected for subsequent research.

Comparison of modified activated carbon and original activated carbon

There are two purposes for using nitric acid to modify activated carbon: (1) to remove impurities from the surface and pore diameter of activated carbon. (2) Nitrates in nitric acid can provide more adsorption sites for subsequent loads. The best modification conditions are: nitric acid concentration of 8 mol/L, microwave heating temperature of 700 °C. The specific surface area was 940 m^2/g, which was 263% higher than the original activated carbon. Using activated carbon after nitric acid activation as the carrier to load manganese dioxide and synthesize MnO_2-AC material can improve the load of manganese dioxide. Activated carbon before activation is shown in Figure 3(a). There are many impurities on the surface of activated carbon, the pores are blocked by impurities, and the specific surface area of activated carbon is small. The activated carbon before activation is shown in Figure 3(b). The impurities on the surface of activated carbon are removed and the pore diameter is increased. Meanwhile, the pore diameter of activated carbon is slightly larger than before due to heating, which is conducive to the increase of specific surface area of activated carbon and the load of manganese dioxide.

SEM characterization of MnO_2-AC and modified activated carbon

Figure 4(a) and 4(b) are the modified activated carbon. It can be observed that the surface of activated carbon is clean, free of impurities and rich in pore diameter. In the preparation process, potassium permanganate is fully absorbed by the activated carbon at first. After the solution fades, drop by drop manganese sulfate solution is added and manganese dioxide is precipitated in the pore diameter of the activated carbon to prevent the flocculation of manganese dioxide (Xu *et al.* 2013). Meanwhile, manganese dioxide is loaded on the activated carbon. The SEM image is shown in Figure 4(c); it is obvious that MnO_2 is generated in the aqueous solution and adsorbed in the pore structure of activated carbon (You *et al.* 2017). At the same time, it can be observed that the pore distribution of activated carbon is uniform and the structure is dense. As shown in Figure 4(d), manganese dioxide particles are evenly distributed on the activated carbon and their size is much smaller than the pore size of activated carbon. Therefore, loading manganese dioxide on activated carbon can effectively avoid the flocculation of manganese dioxide (Zhang *et al.* 2014).

BET analysis

In this study, the S_{BET} of MnO_2-AC was calculated by N_2 adsorption-desorption isotherms (Figure 5), and its surface structure parameters are shown in Table 1. As can be seen from the table, the S_{BET} of activated carbon modified by nitric acid has been greatly improved compared with that of commercially activated carbon. As the pore structure of MnO_2-AC is blocked by nano-manganese dioxide particles, the S_{BET} of MnO_2-AC is reduced compared with activated carbon modified by nitric acid (Zhang *et al.* 2017).

The average pore size of activated carbon and MnO_2-AC treated with nitric acid is 1.239 nm and 0.942 nm, respectively, and the micropore surface area is 0.246 mL/g and 0.197 mL/g, respectively. Compared with the commercially available activated carbon, the pore size is reduced and

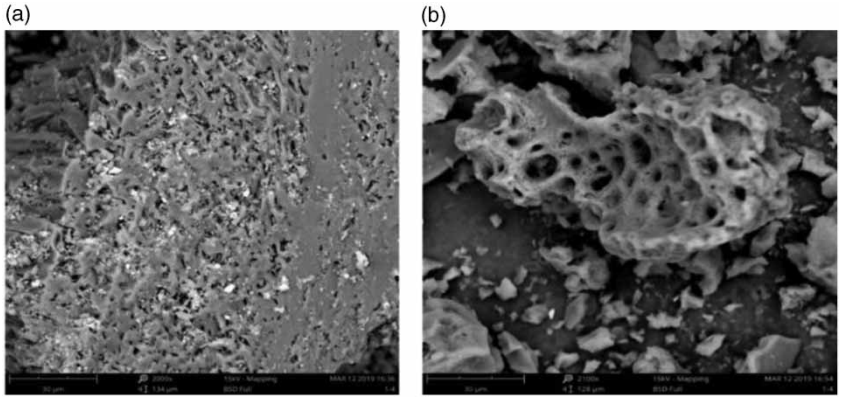

Figure 3 | (a) Original activated carbon, (b) Modified activated carbon.

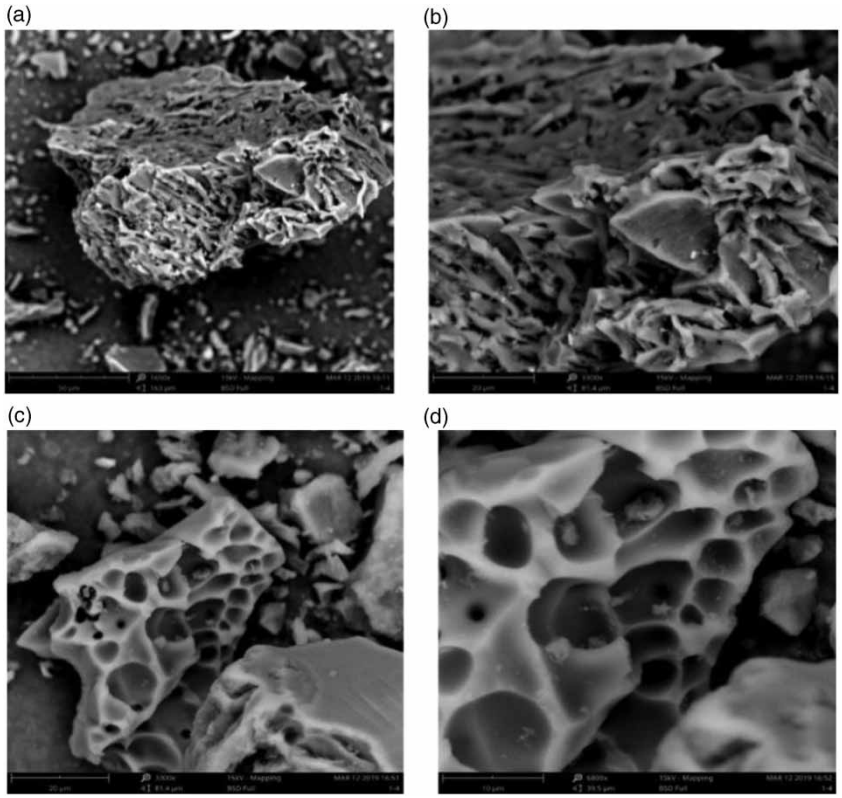

Figure 4 | SEM characterization of MnO_2-AC.

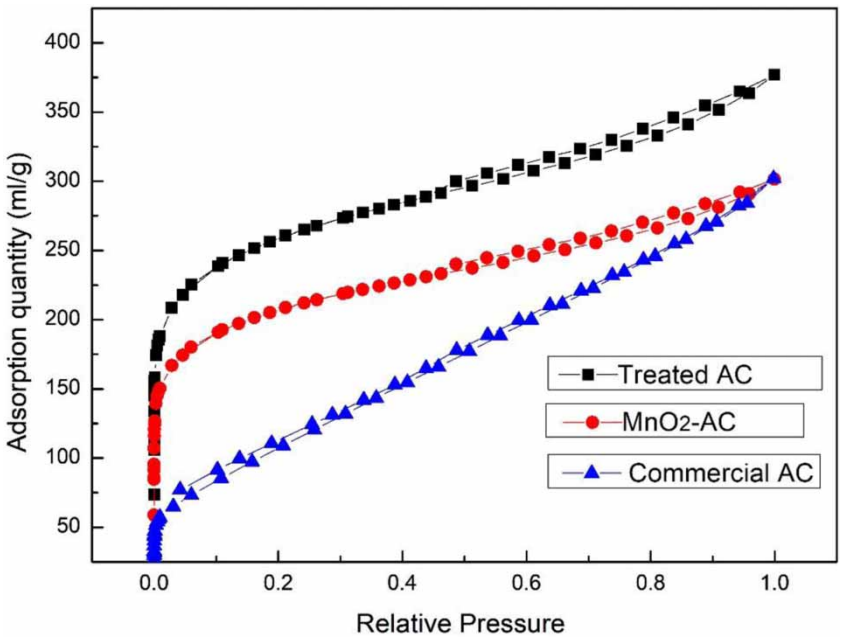

Figure 5 | Nitrogen adsorption and desorption.

the proportion of micropores is increased, which indicates that the pore structure of activated carbon is more abundant after nitric acid modification. MnO_2-AC also has the same characteristics (Zhang *et al.* 2016). Because manganese dioxide is loaded on activated carbon, its average pore size is smaller (Zhou *et al.* 2018).

Table 1 | The pore structure parameters

Absorbent	Treated AC	MnO_2-AC	Commercial AC
S_{BET} (m^2/g)	940.996	752.797	396.219
Micropore area (m^2/g)	604.918	483.934	0
Total pore volume (mL/g)	0.5830	0.4664	0.4674
Micropore volume (mL/g)	0.246	0.197	0
Average pore size (nm)	1.239	0..942	2.359e

Figure 6 shows the pore size distribution of the three activated carbons. It is obvious that nitric acid-modified activated carbon and MnO_2-AC have a more microporous structure, while commercial activated carbon has almost no microporous structure.

Comparison of Pb(II) adsorption by three kinds of activated carbon

Figure 7 depicts the maximum adsorption capacity of three kinds of activated carbon to Pb(II). The maximum adsorption capacity of the original activated carbon is 56 mg/g, the maximum adsorption capacity of nitric acid-modified activated carbon is 363 mg/g, and the maximum adsorption capacity of the MnO_2-AC is 740 mg/g. The modification by nitric acid and load of MnO_2 can significantly improve the adsorption capacity of activated carbon to Pb(II). Compared with the original activated carbon, the maximum adsorption capacity of nitric acid-modified activated carbon can be increased by 5 times, while MnO_2-AC can be increased by about 14 times. This shows that MnO_2-AC can greatly improve the adsorption capacity of activated carbon to Pb(II). The following research focuses on MnO_2-AC, studying the conditions affecting its adsorption and exploring the adsorption mechanism.

Effect of pH on adsorption of Pb(II)

The pH value is one of the important factors affecting the adsorption process, which will affect the surface properties of the adsorbent, the chemical properties of the solution and the morphology of heavy metal ions, so it is of great importance to study the influence of pH value on the adsorption capacity. The effect of solution pH value on lead ion adsorption is shown in Figure 8.

The adsorption capacity of MnO_2-AC on lead ions increases with the increase of solution pH. It reaches its maximum value when pH = 6, and then decreases slowly, and the maximum adsorption value is 664 mg/L. The transition metal oxide surface is rich in hydroxyl groups. At a low pH (pH = 2–6), the surface of the adsorbent is surrounded by a high concentration of hydronium ions, competing with metal ions for the adsorption point. At a low pH, the surface of MnO_2 is highly protonated, making the surface positively charged, thus reducing the material's adsorption capacity and increasing electrostatic repulsion. With the increase of pH value, the adsorbent surface was negative on the whole, and the adsorption capacity of metal ions was enhanced.

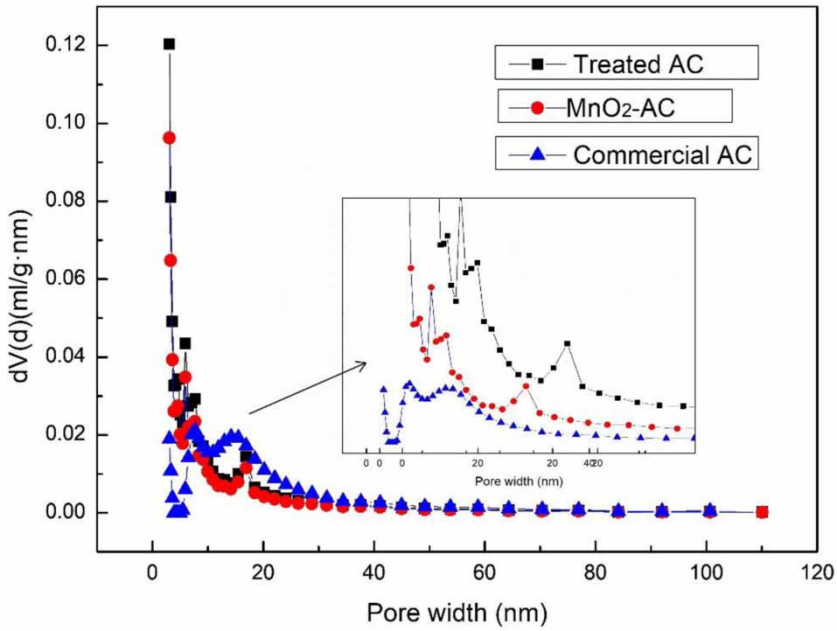

Figure 6 | Pore size distribution.

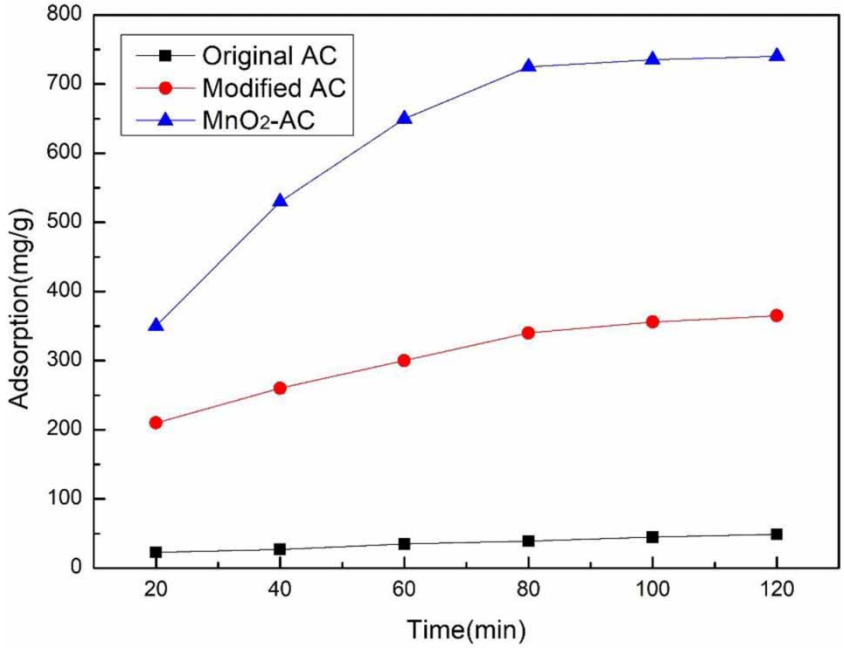

Figure 7 | Pb(II) adsorption by three kinds of activated carbon.

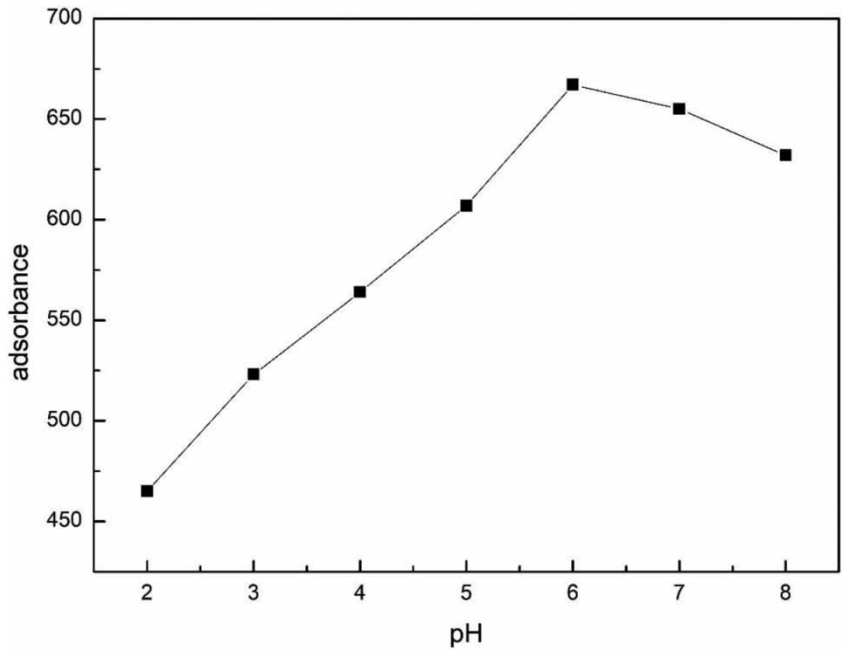

Figure 8 | Effect of pH value on adsorption.

Adsorption studies of lead ions

Figure 9 shows the adsorption equilibrium isothermal curve of the adsorption of Pb(II) by MnO_2-AC. It can be seen from the figure that the adsorption of Pb(II) by MnO_2-AC is rapid at the initial stage, followed by a slow adsorption process. When the lead ion concentration was lower than 300 mg/L, the adsorption amount increased with the increase in concentration. When the lead ion concentration was higher than 300 mg/L, the adsorption capacity of MnO_2-AC increased slowly and gradually became stable, indicating that the adsorption of Pb(II) on its surface tended to be saturated. After calculation, the maximum adsorption capacity of MnO_2-AC for the lead ions is 667 mg/g.

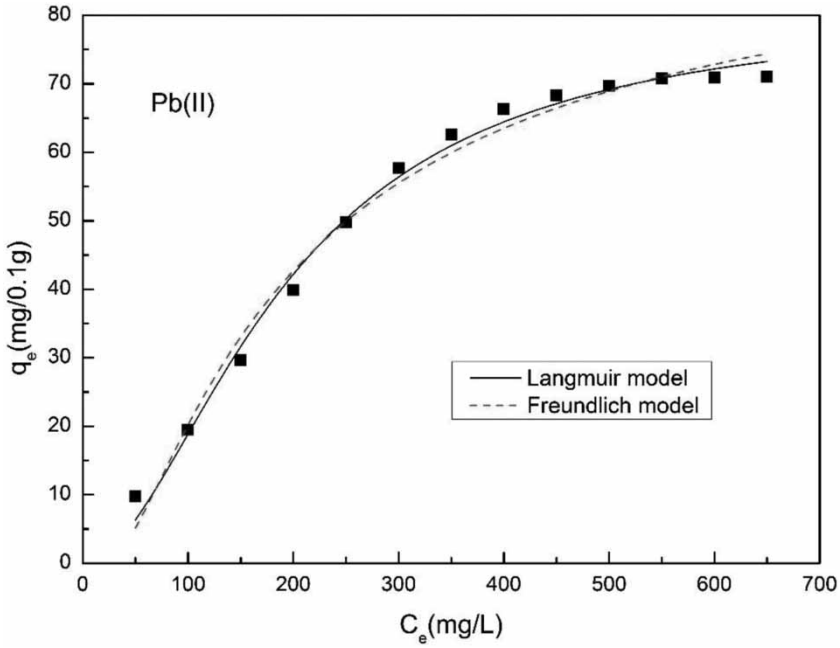

Figure 9 | Adsorption curve fitted by Langmuir and Freundlich model.

In order to clarify the adsorption process and mechanism of lead ions, the adsorption process of Pb(II) by MnO_2-AC was fitted by Langmuir and Freundlich isothermal models (Wu 2007; Yao *et al.* 2010). To clarify the adsorption process and mechanism of lead ions, the adsorption process of Pb(II) by MnO_2-AC was fitted by Langmuir and Freundlich isothermal models. Langmuir isothermal model shows that the adsorption process is monolayer adsorption, and its expression is as follows (Ansoborlo *et al.* 2006):

$$\frac{C_e}{q_e} = \frac{1}{q_{max}K_L} + \frac{1}{q_{max}}C_e \tag{2}$$

The Freundlich model shows that the adsorption process is multi-layer adsorption, and the expression is as follows (Sitko *et al.* 2013):

$$logq_e = logK_F + \frac{1}{n}logC_e \tag{3}$$

where, q_e refers to the adsorption amount (mg/g) of MnO_2-AC on Pb(II) when the adsorption reaches equilibrium, C_e refers to the concentration of Pb(II) in the solution with large equilibrium, q_{max} is the maximum adsorption amount (mg/g) of MnO_2-AC on Pb(II), K_L, 1/n, and K_F are the adsorption constants of the two models respectively.

Table 2 is the fitting parameters of two isothermal models Langmuir and Freundlich for the adsorption Pb(II) of MnO_2-AC. The correlation coefficient R^2 of Langmuir and Freundlich isothermal model and adsorption curve fitting were 0.9917 and 0.9825, respectively. The closer the correlation coefficient is to 1, the higher the fit. Therefore, the adsorption of Pb(II) by MnO_2-AC was more consistent with the Langmuir model, and its adsorption mechanism was single-layer adsorption. The maximum adsorption capacity of MnO_2-AC for Pb(II) was calculated by the Langmuir model fitting as 667 mg/g. Compared with the adsorbents adsorbed by Pb(II) in previous studies, the MnO_2-AC in this study has certain advantages and can be used as an efficient adsorbent for the removal of heavy metal ions in water.

Adsorption kinetics study

The adsorption process of MnO_2-AC on Pb (II) changed with time, as shown in Figure 7. It can be seen that the adsorption curve had a rapid growth period in the early stage, followed by slow growth, and finally reached a stable period around 120 min. Compared with some adsorbents in previous studies, the adsorption capacity of Pb(II) adsorbed by MnO_2-AC within 90 min was much higher. In the whole adsorption process, the rapid adsorption stage is due to the high concentration of lead ions in the solution, which is easy to diffuse to the adsorbent surface and be absorbed. As the adsorption progresses, the solution concentration decreases, the negative functional groups and pores of the adsorbent are occupied by lead ions, the surface of the adsorbent is

Table 2 | Isothermal parameters for Pb(II)

		Langmuir			Freundlich		
Adsorbent	**Metal ion**	q_{max}	K_L	R^2	1/n	K_F	R^2
MnO_2-AC	Pb(II)	667	0.0071	0.9917	0.6489	10.31	0.9825

positively charged, the electrostatic repulsion increases, and the adsorption point position decreases, resulting in the decrease of the adsorption rate. In addition, the adsorption capacity of MnO_2-AC on Pb(II) was about 3 times and 5.5 times of that of modified activated carbon and commercially available activated carbon respectively, and the adsorption performance was significantly improved. This result was consistent with the research results in the adsorption isotherm, proving that MnO_2 modified activated carbon could effectively improve the removal effect of Pb(II). In this study, the pseudo-second-order model and intra-particle diffusion model were used to analyze the adsorption kinetics of Pb(II) with MnO_2-AC (Wu *et al.* 2009; Robati 2013). Where the expression equation of the pseudo-second order dynamics model is as follows (Boudrahem *et al.* 2009):

$$\frac{t}{q_t} = \frac{1}{K_2 q_e^2} + \frac{1}{q_e} t \tag{4}$$

And the intra-particle diffusion model is as follows (Wu *et al.* 2009):

$$q_t = K_{id} t^{0.5} \tag{5}$$

where, q_t represents the adsorption amount (mg/g) of MnO_2-AC on Pb(II) at time t; q_e represents the adsorption amount (mg/g) after reaching the adsorption equilibrium; K_2 and k_{id} are the two kinetic constants. The fitting results of the pseudo-second order dynamic model are shown in Figure 10, and the relevant parameters are shown in Table 3. The adsorption equilibrium capacity ($q_{e,exp}$, mg/g) of MnO_2-AC for Pb(II) was similar to that obtained by fitting ($q_{e,cal}$ mg/g). In addition, the fitting degree R^2 was greater than 0.99, indicating that the adsorption of Pb(II) by MnO_2-AC over time could be explained by the pseudo-second-order kinetic model. The model can also be used to analyze the limiting phase of adsorption. As can be seen from Figure 11, the adsorption of Pb(II) by MnO_2-AC can be divided into two stages. In the initial stage, the diffusion rate constant is the maximum, and then the rate decreases until the adsorption reaches dynamic equilibrium (Van Benschoten *et al.* 1992).

This is consistent with the fitting results and analysis of the pseudo-second-order kinetic model: in the initial stage of rapid adsorption ($k_{i.1}$), more than 50% of Pb(II) in the solution was adsorbed at the surfactant sites of the adsorbent. Secondly, the adsorption rate ($k_{i.2}$) of the second stage decreased significantly, and the removal rate of metal ions was close to the

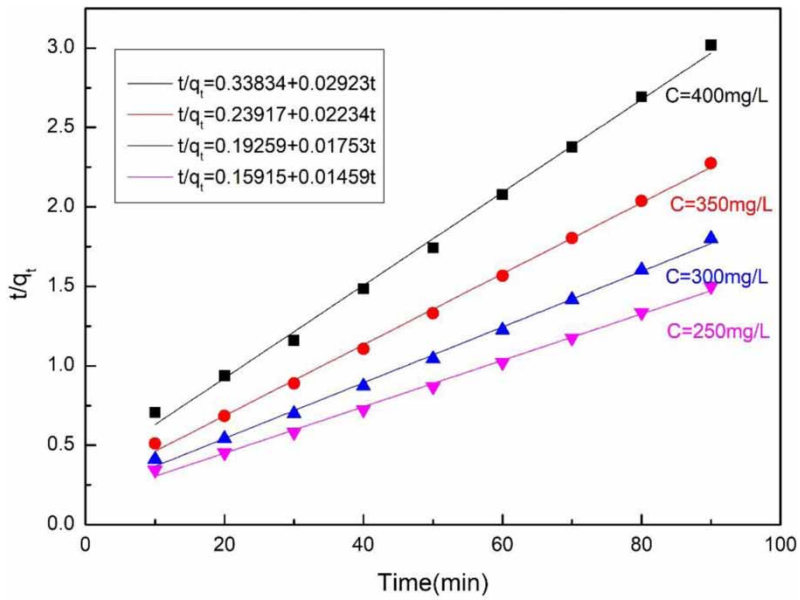

Figure 10 | Pseudo-second-order model.

Table 3 | Kinetic parameters of Pb(II)

Concentration of Pb(II) (mg/g)	Quasi-second order dynamics model				Intraparticle diffusion model			
	$q_{e,exp}$	$q_{e,cal}$	R^2	$K_{i,1}$	R^2	$K_{i,1}$	R^2	$K_{i,2}$
250	48.5	49.8	0.9985	0.015	0.9986	5.26	0.9941	0.82
300	51.2	59.3	0.9992	0.018	0.9951	6.99	0.9895	0.83
350	66.3	65.8	0.9987	0.022	0.9937	8.24	0.9938	0.88
400	67.8	67.7	0.9986	0.029	0.9925	9.29	0.9897	1.29

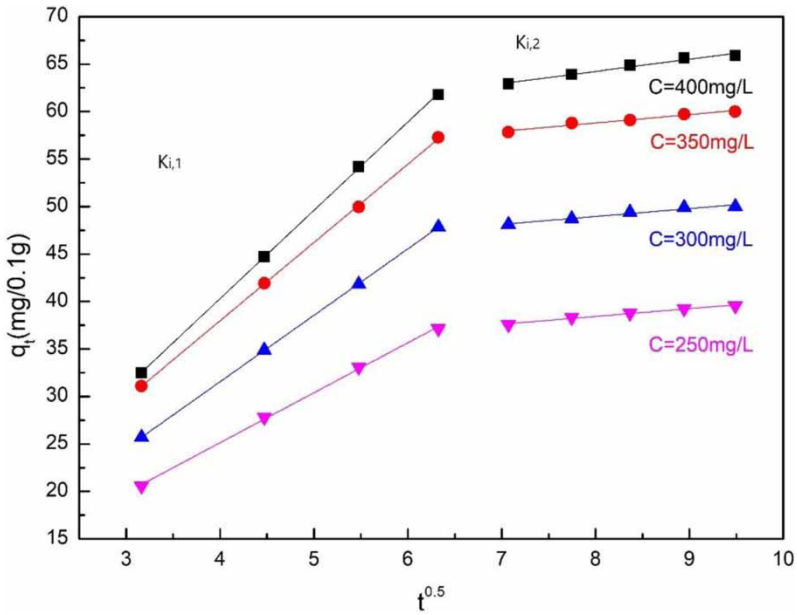

Figure 11 | Intraparticle diffusion model.

maximum. This may be due to the adsorption process of metal ions entering the internal pore structure of the adsorbent, and the ions entering the micropores of the adsorbent. The diffusion resistance also increases with the increase of metal ions, and the adsorption gradually increases.

MnO_2-AC has a more complex pore structure than the modified activated carbon and commercial activated carbon. Due to the loading performance of manganese dioxide, MnO_2-AC has higher activity and finer distribution volume, which can help to make good contact with metal ions and reduce metal ions. Resistant to solution diffusion, these results indicate that manganese dioxide is effective for the modification of activated carbon (Chen & Yeh 2005).

XRD analysis

X-ray diffraction spectrum analysis is used to study the crystal phase and structure of the adsorbent. The X-ray diffraction pattern before and after the modification of activated carbon by manganese dioxide and after the adsorption of Pb(II) by MnO_2-AC is shown in Figure 12. The X-ray diffraction pattern of MnO_2-AC shows multiple peaks, namely C and MnO_2, which are located in 18.10, 26.50, 37.50, 39.000, 40.20, 49.80, 60.3 and 65.1. It can be observed that after manganese dioxide is loaded on the activated carbon, all the diffraction peaks except the carbon peak all point to manganese dioxide (JCPDS No.44-0141).

After the adsorption of lead ions, there was a significant peak of lead ions (JCPDS No.23-0345). This indicates that lead ions are adsorbed on the surface of MnO_2-AC. In order to further explore the adsorption mechanism, infrared analysis is carried out on lead ions (Kim *et al.* 2013; Yuan *et al.* 2014).

FTIR analysis

The infrared spectra before and after the adsorption of Pb(II) by MnO_2-AC are shown in Figure 13. In the case of MnO_2-AC, the spectrum showed absorption bands of 1,386.36,

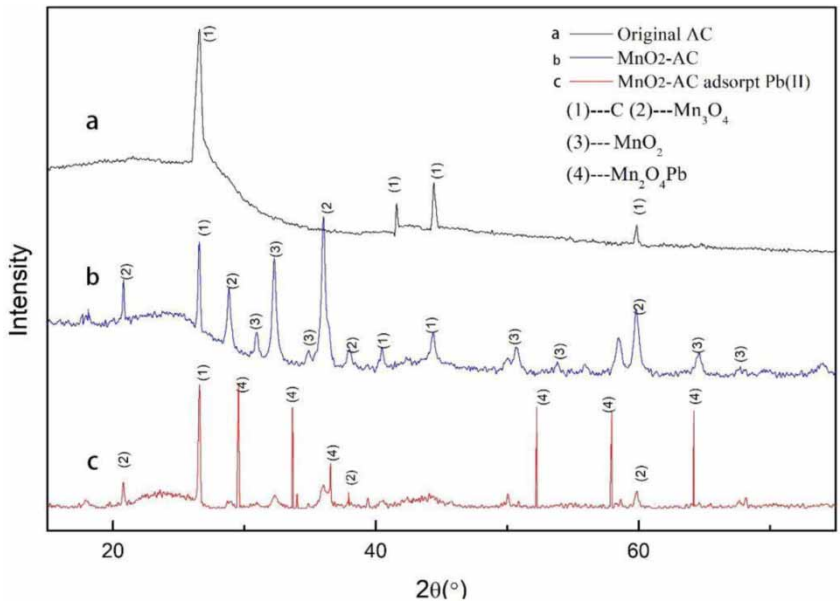

Figure 12 | XRD spectrum.

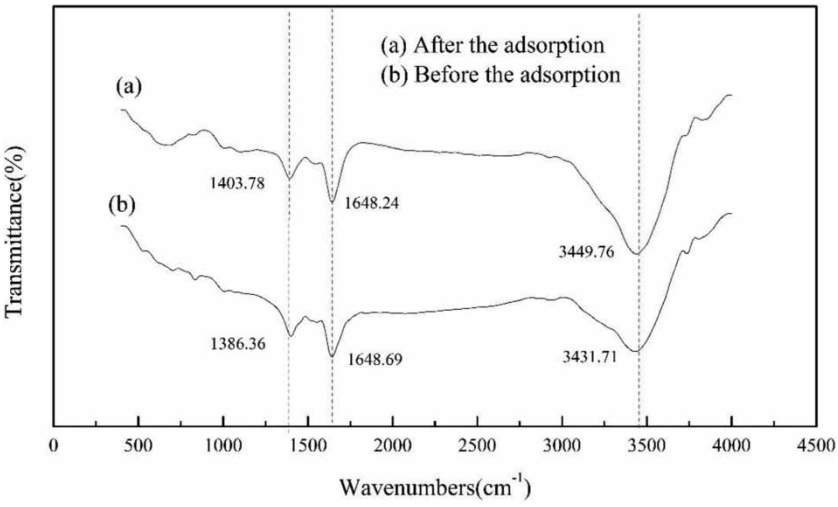

Figure 13 | FTIR spectrum.

1,648.69 and 3,431.71 cm^{-1}. The peak at 1,386.36 cm^{-1} can be attributed to the vibration of the combination of hydroxyl group and manganese atoms; the peak value at 1,648.69 cm^{-1} was attributed to the bending vibration of the C-C bond; the widened band at 3,431.71 cm^{-1} can be attributed to the bending vibration of the adsorbed molecular water and the stretching vibration of the hydroxyl group. After adsorption of Pb(II) by MnO_2-AC, the hydroxyl bands containing Pb molecules were significantly shifted from 3,431.71 and 1,386.36 cm^{-1} to 3,449.76 and 1,403.78 cm^{-1}, as shown in the figure. The observation results show that the interaction between metal ions and hydroxyl groups on the surface of the adsorbent can achieve the effect of adsorbing metal ions. At the same time, the significant movement of the hydroxyl band may be attributed to the formation of the spherical complex between heavy metal ions and manganese dioxide, forming the Mn-O-Pb bond.

XPS analysis

XPS was used to analyze the chemical composition and structural changes of MnO_2-AC before and after adsorption of lead ions. The XPS spectra of lead ion adsorption by MnO_2-AC are shown in Figure 14(a), with 284.8 eV, 532.4 eV, 642.3 eV and 654.1 eV, 143.3 eV and 137.8 eV. The corresponding elements at the crest are C1s, O1s,

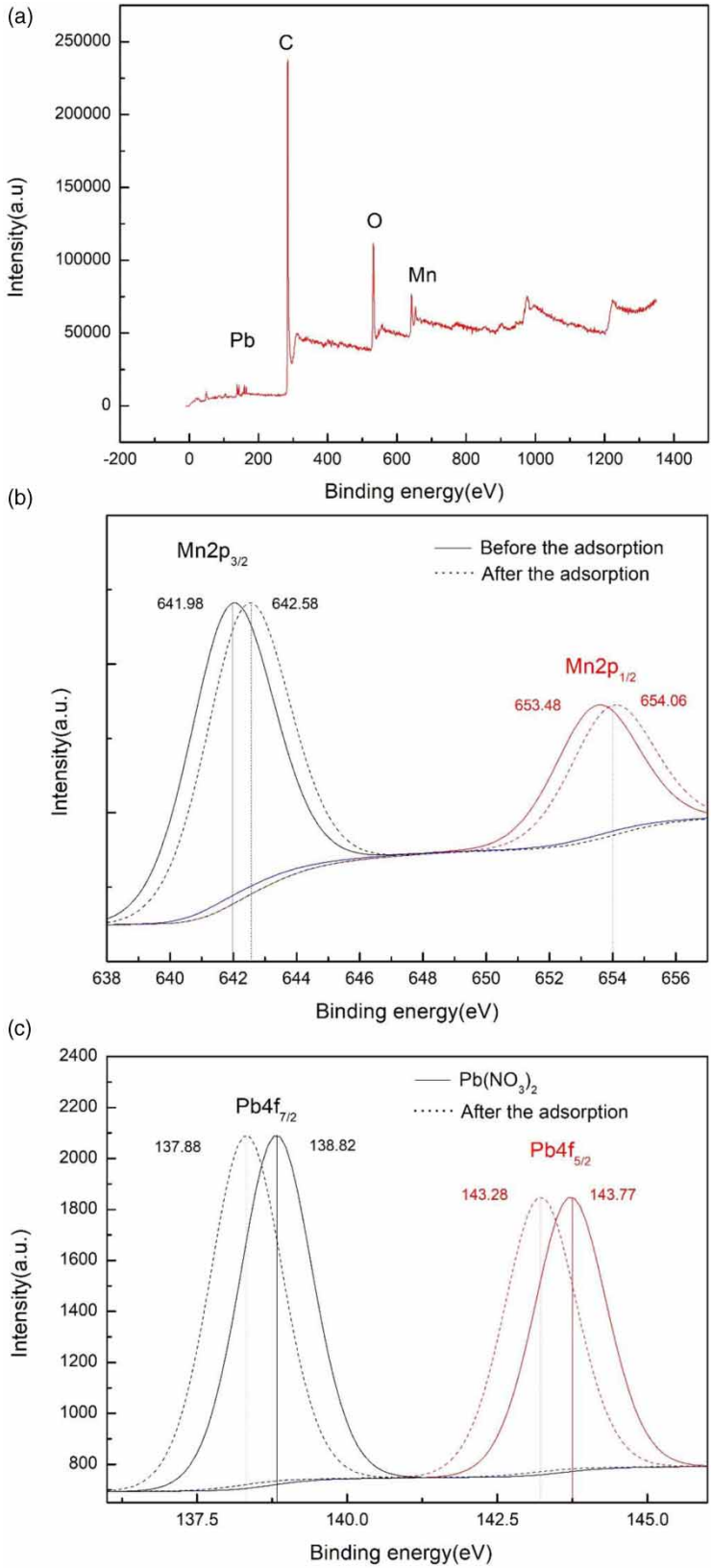

Figure 14 | (a) XPS wide-scan spectrum, (b) XPS scan of MnO_2 before and after adsorption for Pb(II), (c) XPS scan of Pb(II) before and after adsorption for Pb(II).

$Mn2p_{3/2}$ and $Mn2p_{1/2}$, $Pb_{5/2}$ and $Pb_{7/2}$, respectively. It is noted that after the adsorption of Pb(II) by MnO_2-AC, the binding energy of Mn increases with adsorption (Kushwaha *et al.* 2012). As shown in Figure 14(b), after adsorption of Pb(II), the binding energy of MnO_2-AC at Mn increased from 641.98 and 653.48 eV to 642.3 and 654.1 eV, respectively. This may be the result of the Mn-O-Pb bond formed on the surface of the adsorbent, resulting in a decrease in the density of the electron cloud outside the nucleus around Mn atoms, thus increasing the binding energy of Mn2p. As shown in Figure 14(c), it was also observed that the binding energy of Pb4f in $Pb(NO_3)_2$ was 138.82 and 143.77 eV, respectively. After adsorption, the binding energy decreased to 137.88 and 143.28 eV, respectively, and the transition from the high to low region was obvious, indicating that there was a specific interaction between Pb(II) and MnO_2-AC. In addition, the peak observed at 137.88 eV was consistent with the Pb-O bond at 138.0 eV, further confirming that Pb(II) and manganese dioxide in MnO_2-AC formed an intraplate complex. No clear evidence of Pb(II) being oxidized into Pb(IV) or forming other solid phases was observed from the XPS spectrum, indicating that the main mechanism of MnO_2-AC removing Pb(II) was attributed to adsorption (Fiedor *et al.*1998; Sofer *et al.* 2014).

CONCLUSION

This paper compared the adsorption capacity of Pb(II) on original activated carbon, modified activated carbon and manganese dioxide-doped activated carbon, and the results showed that the modified nitric acid activated carbon can significantly improve the adsorption capacity of Pb(II) on the activated carbon, while the modified activated carbon doped by manganese dioxide can further improve the adsorption capacity of lead ions. The optimal doping ratio of manganese dioxide on activated carbon was explored, the molar ratio was $AC:MnO_2 = 1:0.1$. The effect of pH on adsorption was also explored, the results showed that the maximum adsorption capacity of MnO_2-AC on Pb(II) increased with the increase of pH value, and reached the maximum adsorption capacity when pH was 6, and then decreased with the continued increase of pH value.

In order to study the adsorption principle of MnO_2-AC on Pb(II), this paper explored the adsorption kinetics of MnO_2-AC on Pb(II), and conducted XRD, XPS and FTIR tests on the samples before and after Pb(II) adsorption. The principle of adsorption can be divided into two parts. When the concentration of lead ions in solution is high, the adsorption of Pb(II) by MnO_2-AC is in the sphere, and a large number of manganese dioxide particles in the apertures of activated carbon have a negative charge. After electrostatic adsorption of Pb(II), it is fixed in the structure of activated carbon. With saturation of adsorption, the adsorption rate of Pb(II) gradually decreases. At this time, the main adsorption principle is internal diffusion of ions, and Pb(II) is mainly fixed by electrostatic adsorption.

ACKNOWLEDGEMENTS

The authors would like to express their gratitude to the Specialized Research Fund for the National Natural Science Foundation of China (21966019), Yunnan Ten Thousand Talents Plan Industrial Technology Talents Project (2019-1096), Yunnan Ten Thousand Talents Plan Young & Elite Talents Project (2018–73), Yunnan Science and Technology Planning Project (2018IB020), Yunnan Science and Technology Planning Project (2018IC085).

DATA AVAILABILITY STATEMENT

All relevant data are included in the paper or its Supplementary Information.

REFERENCES

Ansoborlo, E., Prat, O., Moisy, P., Den Auwer, C., Guilbaud, P. & Carriere, M. 2006 Actinide speciation in relation to biological processes. *Biochimie* **88** (11), 1605–1618.

Boudrahem, F., Aissani-Benissad, F. & Aiet-Amar, H. 2009 Batch sorption dynamics and equilibrium for the removal of lead ions from aqueous phase using activated carbon developed from coffee residue activated with zinc chloride. *Journal of Environmental Management* **90** (10) (suppl.3), 3031–3039.

Chansuvarn, W. & Jainae, K. 2017 Adsorptive removal of lead(II) ions from aqueous solution onto chemical modified autoclaved aerated concrete. *Applied Mechanics and Materials* **866**, 119–123.

Chen, J. J. & Yeh, H. H. 2005 The mechanisms of potassium permanganate on algae removal. *Water Research* **39** (18), 4420–4428.

Fiedor, J. N., Bostick, W. D., Jarabek, R. J. & Farrell, J. 1998 Understanding the mechanism of uranium removal from groundwater by zero-valent iron using X-ray photoelectron spectroscopy. *Environmental Science & Technology* **32** (10), 1466–1473.

Khushk, S., Zhang, L., Li, A., Irfan, M. & Zhang, X. 2020 Microwave-assisted hydrothermal carbonization of furfural residue for adsorption of Cr(vi): adsorption and kinetic study. *Polish Journal of Environmental Studies* **29** (2), 1–11.

Kim, E. J., Lee, C. S., Chang, Y. Y. & Chang, Y. S. 2013 Hierarchically structured manganese oxide-coated magnetic nanocomposites for the efficient removal of heavy metal ions from aqueous systems. *ACS Applied Materials & Interfaces* **5** (19), 9628–9634.

Kushwaha, S., Sreedhar, B. & Padmaja, A. P. 2012 XPS, EXAFS, and FTIR as tools to probe the unexpected adsorption-coupled reduction of u(vi) to u(v) and u(iv) on *borassus flabellifer*-based adsorbents. *Langmuir* **28** (46), 16038–16048.

Langmuir, I. 1917 The constitution and fundamental properties of solids and liquids. II. Liquids. *Journal of the American Chemical Society* **39**, 1848–1906.

Mallakpour, S. & Motirasoul, F. J. U. S. 2018 Ultrasonication synthesis of PVA/PVP/α-MnO_2 -stearic acid blend nanocomposites for adsorbing Cd II ion. *Ultrasonics Sonochemistry* **40**, 410–418.

Manes, M. & Hofer, L. J. E. 1982 Application of the Polanyi adsorption potential theory to adsorption from solution on activated carbon. *Chemischer Informationsdienst* **13** (5), 4216–4221.

Mishra, S. P., Dubey, S. & Tiwari, D. 2004 Inorganic particulates in removal of heavy metal toxic ions. Rapid and efficient removal of Hg(II) by hydrous manganese and tin oxides. *Journal of Colloid and Interface Science* **279**, 61–67.

Peng, L., Zeng, Q., Tie, B., Lei, M., Yang, J., Luo, S. & Song, Z. 2015 Manganese dioxide nanosheet suspension: a novel absorbent for cadmium (II) contamination in waterbody. *Journal of Colloid and Interface Science* **456**, 108–115.

Pera-Titus, M., GarcíA-Molina, V., Baños, M. A., Giménez, J. & Esplugas, S. J. A. C. B. E. 2004 Degradation of chlorophenols by means of advanced oxidation processes: a general review. *Applied Catalysis B-Environmental* **47**, 219–256.

Pourjavid, M. R., Sehat, A. A., Arabieh, M., Yousefi, S. R., Hosseini, M. H. & Rezaee, M. 2014 Column solid phase extraction and flame atomic absorption spectrometric determination of manganese(II) and iron(III) ions in water, food and biological samples using 3-(1-methyl-1H-pyrrol-2-yl)-1H-pyrazole-5-carboxylic acid on synthesized graphene oxide. *Materials Science & Engineering C-Materials for Biological Applications* **35**, 370–378.

Robati, D. 2013 Pseudo-second-order kinetic equations for modeling adsorption systems for removal of lead ions using multi-walled carbon nanotube. *Journal of Nanostructure in Chemistry* **3** (1), 55.

Sellaoui, L., Kehili, M., Lima, E. C., Bonilla-Petriciolet, A. & Erto, A. 2019 Adsorption of phenol on microwave-assisted activated carbons: modelling and interpretation. *Journal of Molecular Liquids* **274**, 309–314.

Sitko, R., Turek, E., Zawisza, B., Malicka, E., Talik, E. & Heimann, J. R. 2013 Adsorption of divalent metal ions from aqueous solutions using graphene oxide. *Dalton Transactions* **42** (16), 5682.

Sofer, Z., Jankovský, O., Simek, P., Klimova, K., Mackova, A. & Pumera, M. 2014 Uranium- and thorium-doped graphene for efficient oxygen and hydrogen peroxide reduction. *ACS Nano* **8**, 7106–7114.

Tangahu, B. V., Abdullah, S., Rozaimah, S., Basri, H., Idris, M., Anuar, N. & Mukhlisin, M. 2011 A review on heavy metals (As, Pb and Hg) uptake by plants through phytoremediation. *International Journal of Chemical Reactor Engineering* **2011**, 1–31.

Van Benschoten, J. E., Lin, W. & Knocke, W. R. 1992 Kinetic modeling of manganese(ii) oxidation by chlorine dioxide and potassium permanganate. *Environmental Science & Technology* **26** (7), 1327–1333.

Wan, S., He, F., Wu, J., Wan, W., Gu, Y. & Gao, B. 2016 Rapid and highly selective removal of lead from water using graphene oxide-hydrated manganese oxide nanocomposites. *Journal of Hazardous Materials* **314** (15), 32–40.

Wang, M. C., Sheng, G. D. & Qiu, Y. P. 2015 A novel manganese-oxide/biochar composite for efficient removal of lead(ii) from aqueous solutions. *International Journal of Environmental Science & Technology* **12** (5), 1719–1726.

Wang, M., Shen, M., Zhang, L., Tian, J., Jin, X., Zhou, Y. & Shi, J. 2017 2D-2D MnO_2/g-C_3N_4 heterojunction photocatalyst: in-situ synthesis and enhanced CO_2 reduction activity. *Carbon* **120**, 23–31.

Wu, C. H. 2007 Adsorption of reactive dye onto carbon nanotubes: equilibrium, kinetics and thermodynamics. *Journal of Hazardous Materials* **144** (1–2), 93–100.

Wu, F. C., Tseng, R. L. & Juang, R. S. 2009 Initial behavior of intraparticle diffusion model used in the description of adsorption kinetics. *Chemical Engineering Journal* **153** (1–3), 1–8.

Xu, M., Wang, H., Di, L., Qu, D., Zhai, Y. & Wang, Y. 2013 Removal of Pb(II) from aqueous solution by hydrous manganese dioxide: adsorption behavior and mechanism. *Journal of Environmental Sciences-China* **25**, 479–486.

Yao, Y., Xu, F., Chen, M., Xu, Z. & Zhu, Z. 2010 Adsorption behavior of methylene blue on carbon nanotubes. *Bioresource Technology* **101** (9), 3040–3046.

You, X., Cao, J., Liu, X., Lu, J. & Chen, X. 2017 Synthesis of the poly (acrylic acid acrylic sodium) bentonite composite and its adsorption of Cd(II). *Asi-Pacific Journal of Chemical Engineering* **12**, 65–74.

Yuan, L. Y., Bai, Z. Q., Zhao, R., Liu, Y. L., Li, Z. J. & Chu, S. Q. 2014 Introduction of bifunctional groups into mesoporous silica for enhancing uptake of thorium(iv) from aqueous solution. *ACS Applied Materials & Interfaces* **6** (7), 4786–4796.

Zhang, D. D., Zhao, D. L., Zhang, J. M. & Bai, L. Z. 2014 Microwave absorbing property and complex permittivity and permeability of graphene-cds nanocomposite. *Journal of Alloys and Compounds* **589**, 378–383.

Zhang, W., Wang, F., Wang, P., Lin, L., Zhao, Y. & Zou, P. W. 2016 Facile synthesis of hydroxyapatite/yeast biomass composites and their adsorption behaviors for lead (ii). *Journal of Colloid and Interface Science* **477**, 181–190.

Zhang, H., Gu, L., Zhang, L., Zheng, S., Wan, H. & Sun, J. 2017 Removal of aqueous Pb(II) by adsorption on Al_2O_3-pillared layered MnO_2. *Applied Surface Science* **406**, 330–338.

Zhou, Q., Liao, B., Lin, L., Qiu, W. & Song, Z. 2018 Adsorption of Cu(ii) and Cd(ii) from aqueous solutions by ferromanganese binary oxide-biochar composites. *Science of The Total Environment* **615**, 115–122.

First received 11 April 2020; accepted in revised form 16 July 2020. Available online 29 July 2020